Space-vector State Dynamic Model of the SynRM Considering Self, Cross-Saturation and Iron Losses and Related Identification Technique

Angelo Accetta, *Member IEEE,* Maurizio Cirrincione, *Senior Member IEEE,* Marcello Pucci, *Senior Member IEEE,* and Antonino Sferlazza, *Member IEEE.*

***Abstract*—This paper proposes a space-vector dynamic model of the Synchronous Reluctance Motor (SynRM) including both self-saturation, cross-saturation effects, and iron losses. The model is expressed in state form, where the magnetizing current has been selected as a state variable. The proposed dynamic model is based on an original function between the stator flux and the magnetizing current components, improving a previously developed magnetic model. Additionally, the proposed model includes, besides the magnetic saturation, also iron losses. The proposed model requires 11 coefficients, among which 6 describe the self-saturation on both axes and 5 describe the cross-saturation. This paper presents also, from one side a technique for the estimation of the parameters of the magnetic model, and from the other side a purposely developed methodology for measuring the iron losses resistance as well as its variation with the speed and stator current amplitude. The proposed parameter estimation technique has been tested in both numerical simulation and experimentally on a suitably developed test set-up and the proposed model has been thus validated experimentally**

***Index Terms*—Synchronous Reluctance Motor (SynRM), space-vector dynamic model, magnetic model, iron losses, parameters' estimation**

I. Introduction

In the last years, Synchronous Reluctance Motors (SynRMs) have proved to be a good alternative to both Induction Motors (IMs) and Permanent Magnet Synchronous Motors (PMSMs) [2]–[4] thanks to their features of simplicity, robustness, and cheapness. On the one hand, they do not present rotor joule losses, as in the IM case, on the other hand, they do not require expensive permanent magnets on the rotor, as in the PMSM case. Moreover, they offer overload capability and high dynamical performance [5]–[7].

As for the SynRM controllability and related dynamical performance, it is highly dependent on its proper dynamic modeling. From this point of view, the proper representation of the magnetic behavior of the machine, including both self and cross-saturation, is crucial. The definition of the flux versus current characteristics (or the current versus flux ones) of the magnetic model and the identification of the related parameters have been addressed in the scientific literature [8]–[14].

As for the dynamic model of the SynRM, [15] treats it in terms of its space-vector state formulation with two approaches, assuming either the stator flux or the stator current components as state variables. It also makes an interesting review of the approaches adopted in the scientific literature. If stator currents are assumed as state variables, usually the analytical expressions of the corresponding inductances versus current are provided, derived from the expression of the flux versus current (initially constant and then linearly decreasing). In particular, [16] models the inductance as a piecewise function, while [17] improves it by including the cross-saturation effect, [18] models the inductance by employing polynomials whose 13 coefficients are estimated by least-squares (LS), and finally [19] models the inductance through rational functions requiring 16 coefficients, but presenting the significant drawback of not fulfilling the reciprocity conditions.

More recently, [20], [21] have proposed flux versus current functions based on exponentials. As a further improvement, [22] has proposed a more accurate representation of the cross saturation phenomenon in particular for very low and very high values of the magnetizing current. In detail, the model proposed in [22] is based on hyperbolic functions. In the very recent past, [13] has proposed a physically motivated analytical non-linear flux versus current functions permitting consideration of both self and cross saturation. The model in [13] correctly guarantees the reciprocity conditions to be respected. As for the self-saturation phenomenon, it proposes a combination of the $\tanh(\cdot)$ and a linear function. From this point of view, the approach in [13] is the same already proposed by the authors in [22]. As for the cross-saturation phenomenon, the approach in [13] is only slightly different from that proposed by the authors in [22]. The specific differences are highlighted in Sec. II-D.

If the stator flux is assumed as a state variable, an inductance versus flux function is typically provided, derived from the current versus flux function. In particular, [23] models the current versus flux as a power function and consequently deduces the inductance versus flux function, even if the cross-saturation effect has not been considered. Likewise, [24] models the inductance utilizing an arctangent function depending on 3 coefficients, with the advantage that the coefficients are physically meaningful and therefore the fitting procedure is easier, but with the same disadvantage as [23] since the cross-saturation is neglected. In contrast to these works, [15] proposes a current versus flux augmented power function, so that the cross-saturation can be taken into account, and depending on 9 coefficients: since this approach is based on the current versus flux expression, its coefficients present a less physical meaning.

Finally, [11] addresses a current versus flux approach, where the bivariate approach is introduced to take into account the cross saturation. An effective strategy for determining the polynomial coefficients is proposed as well.

As for the techniques for the magnetic characterization of

10.1109/TIA.2023.3252528 © 2023 IEEE

the SynRM, most of them require the SynRM drive to work at a constant speed, which results in the need for a speed-controlled prime mover drive with 4-quadrant features [25]. Other identification techniques are based either on acceleration tests [26] or on large-signal high-frequency injection at stand-still [27]: both methods are hardly adoptable when the drive cannot be mechanically disconnected from the load. Recently, two interesting solutions have been proposed for SynRM identification with stand-still tests, without the need for locking the rotor [28], [29].

Besides the magnetic saturation, another aspect to be accounted for in modeling SynRMs are the iron losses, which may have a significant effect on the current angles adopted for some control strategies [30]–[37]. As a matter of fact, iron losses cause a phase displacement between the magnetizing and stator currents space vectors, and cause a reduction of the producible electromagnetic torque. Not many papers in the scientific literature treat the inclusion of iron losses in the dynamic model of SynRMs. Besides writing the dynamic voltage equation of the motor, none of these papers, however, express the dynamic model in state form, which is particularly useful for control applications.

This paper tries to fill in these gaps in scientific literature. More specifically, it improves the magnetic model of the SynRM, proposing a more accurate mathematical representation. The magnetic model in [20], [21] has been improved here to better describe the cross saturation phenomenon in the low stator currents region. Moreover, a further improvement of [20], [21] is that the proposed cross saturation model respects the physical condition for which the cross saturation inductance is positive when the stator current components present opposite signs and viceversa [38]. Additionally, as an original contribution and further improvement to [22], the iron losses have been included in the model and the complete state representation of the model including both the magnetic saturation and the iron losses has been developed. Such a theoretical contribution, to the best of the authors' knowledge, is not present in the scientific literature. Finally, this paper proposes a technique for the estimation of the set of parameters of the proposed model. The proposed parameter estimation technique has been tested in both numerical simulation and experimentally on a suitably developed test set-up. The proposed dynamic model has been finally validated experimentally on a suitably devised test set-up.

This paper is an upgrade and an improvement of [39].

II. The Dynamic Model Considering Magnetic Saturation and Iron Losses

Iron losses in SynRMs occur on both the stator and the rotor. The losses in the stator are similar to those in a conventional induction-machine stator. The rotor would ideally have zero losses since the mmf (magnetomotive force) wave rotates at the same angular speed as the rotor. In real motors, however, the rotor can be subjected to high-frequency flux changes as the rotor axial laminations interact with the stator teeth. If the stator is badly designed (i.e., with wide teeth openings) such losses may be considerable [30]. Moreover, space harmonics of the mmf combined with time harmonics of the supply voltage cause further iron losses in the rotor. A very accurate space-vector circuital model of the SynRM including iron losses has been presented in [36], shown in Fig. 1. This complete scheme considers three resistances matrices accounting for the iron losses,

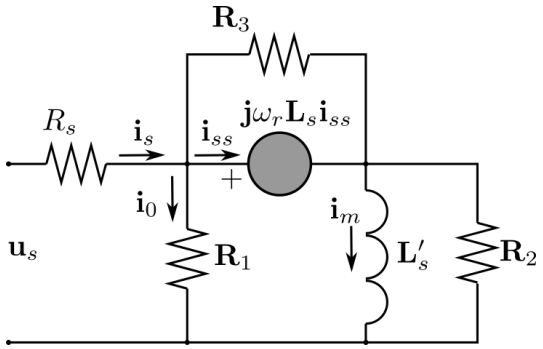

Fig. 1: Complete space-vector circuital model of the SynRM including iron losses

called $\mathbf{R}_1$, $\mathbf{R}_2$, and $\mathbf{R}_3$. As clearly explained in [36], these three resistance matrices are subjected to three different voltage vectors, respectively $d\mathbf{\Psi}_s/dt + \mathbf{j}\omega_r\mathbf{\Psi}_s$, $d\mathbf{\Psi}_s/dt$ and $\mathbf{j}\omega_r\mathbf{\Psi}$. $\mathbf{R}_1$ accounts for the major contribution of iron losses. $\mathbf{R}_2$ represents the transient iron losses. It is reasonable to assume that $\mathbf{R}_1$ is a symmetric matrix, while $\mathbf{R}_2$ is an asymmetric one. In the case of a transverse-laminated rotor $R_{2x} < R_{2y}$ is generally true; on the contrary, for an axially laminated rotor, $R_{2x} > R_{2y}$ is valid, because of eddy currents due to (transient) y-axis excitation, which are not impeded by lamination. Stator harmonics and the slotted structure cause additional losses in the rotor. Since these losses depend on speed, they can be accounted for by the $\mathbf{R}_3$ matrix. This issue has been specifically treated in [37] for an axially laminated rotor. In that case, $R_{3x} = R_{2y}$ was assumed, while R_{3y} and R_{2x} were neglected. As clearly stated in [36], and largely assumed in the scientific literature, steady-state stator harmonics, and slotting can be neglected, $\mathbf{R}_3 \to \infty$, as well as transient iron losses, $\mathbf{R}_2 \to \infty$, leading to the simplified space-vector circuit in Fig. 2 with a unique resistance matrix $\mathbf{R}_0$ that, for the above-cited reasons, can be assumed symmetrical and therefore indicated as a scalar in Fig. 2. Such scalar has been further assumed constant, after the characterization of the SynRM under test (see Fig. 10). For the above explanations, the dynamic model of the SynRM will be developed starting from the simplified electric circuit in Fig. 2.

In Fig. 2, $\mathbf{L}_s$ and $\mathbf{L}'_s$ are respectively the static and dynamic stator inductances matrices, depending on the direct and quadrature components of the magnetizing current i_{mx}, i_{my} and are defined in the following subsection. From Fig. 2 it is clear that, because of the iron losses, the magnetizing current does not coincide with the stator current, in both amplitude and phase, which strongly influences the control action.

A. Magnetic model of the SynRM including cross-saturation

As for the magnetic characteristics of the SynRM, the following functions are proposed, which consider both the self and cross-saturation effects and describe the relationships between the direct and quadrature components of the stator fluxes and the corresponding components of the magnetizing currents in the synchronous reference frame. The stator flux direct x and quadrature y components have been defined as follows:

$$\begin{aligned}\Psi_{sx} &= 2\alpha_1\left(\frac{1}{1+e^{-\beta_1 i_{mx}}} - \frac{1}{2}\right) + \eta_1 i_{mx} + \Delta\Psi_{sx}\\ \Psi_{sy} &= 2\alpha_2\left(\frac{1}{1+e^{-\beta_2 i_{my}}} - \frac{1}{2}\right) + \eta_2 i_{my} + \Delta\Psi_{sy}\end{aligned} \tag{1}$$

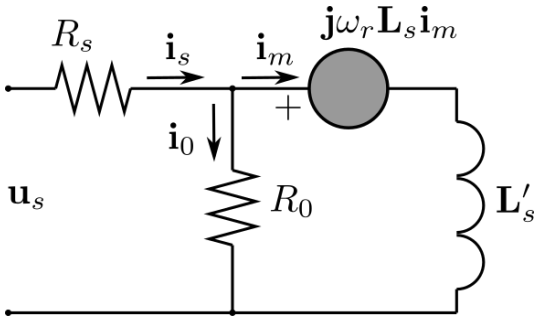

Fig. 2: Simplified space-vector circuital model of the SynRM including iron losses

The first terms of (1) are the self-saturation terms, composed of an exponential term plus a linear one. The self-saturation phenomenon on each axis is described by 3 parameters, namely $\alpha_{1,2}$, $\beta_{1,2}$, and $\eta_{1,2}$.

The cross-saturation flux terms have been derived starting from the following co-energy variation function, whose definition is one of the original contributions of this paper:

$$\begin{aligned}\Delta W' &= f\left(i_{mx}\right) g\left(i_{my}\right) = \\ &= \gamma \frac{1}{1+e^{\left(-\frac{i_{mx}-\mu_1 \operatorname{sgn}(i_{mx})}{\sigma_1}\operatorname{sgn}(i_{mx})\right)}} \\ &\frac{1}{1+e^{\left(-\frac{i_{my}-\mu_2 \operatorname{sgn}(i_{my})}{\sigma_2}\operatorname{sgn}(i_{my})\right)}} = \\ &= \gamma \frac{1}{1+e^{-i_X}} \frac{1}{1+e^{-i_Y}} \end{aligned} \quad (2)$$

where:

$$\begin{aligned} i_X &= \frac{i_{mx}-\mu_1 \operatorname{sgn}\left(i_{mx}\right)}{\sigma_1} \operatorname{sgn}\left(i_{mx}\right) \\ i_Y &= \frac{i_{my}-\mu_2 \operatorname{sgn}\left(i_{my}\right)}{\sigma_2} \operatorname{sgn}\left(i_{my}\right) \end{aligned}$$

From which the cross saturation flux variation terms can be computed as:

$$\begin{aligned} \Delta\Psi_{sx} &= \frac{d\Delta W'}{di_{mx}} = -\frac{\gamma}{\sigma_1} \frac{\operatorname{sgn}\left(i_{mx}\right)}{\left(e^{\frac{i_X}{2}}+e^{-\frac{i_X}{2}}\right)^2} \frac{1}{1+e^{-i_Y}} \\ \Delta\Psi_{sy} &= \frac{d\Delta W'}{di_{my}} = -\frac{\gamma}{\sigma_2} \frac{\operatorname{sgn}\left(i_{my}\right)}{\left(e^{\frac{i_Y}{2}}+e^{-\frac{i_Y}{2}}\right)^2} \frac{1}{1+e^{-i_X}} \end{aligned} \quad (3)$$

The cross saturation phenomenon is described by 5 parameters: γ, σ_1, σ_2, μ_1, μ_2. The above mathematical formulation has been conceived by analyzing Fig. 2 in [8]. This last figure shows that Ψ_{sx} reduces for increasing values of the current i_{sy}. Moreover, for a given value of i_{sx}, the amount of reduction of Ψ_{sx} depends on the absolute value of i_{sy}, being independent of its sign. The higher the absolute value of i_{sy}, the higher the flux reduction on the x-axis. In addition, the same figure shows that the flux variation on the x-axis is null for zero value of i_{sx}, very small for high values of i_{sx}, while it presents a maximum for a certain intermediate range of i_{sx}. These considerations suggest that the flux variation on the x-axis should be weighted with a function of i_{sx} presenting a bell shape.

Since the nonlinear inductor should not generate or dissipate electrical energy, the reciprocity condition must be satisfied [15], [29], and the cross-saturation dynamic inductance can be coherently defined as:

$$\begin{aligned} L'_{sxy} &= \frac{d\Delta\Psi_{sx}}{di_{my}} = \frac{d\Delta\Psi_{sy}}{di_{mx}} = \\ &= -\frac{\gamma}{\sigma_1\sigma_2} \frac{\operatorname{sgn}\left(i_{mx}\right)}{\left(e^{\frac{i_X}{2}}+e^{-\frac{i_X}{2}}\right)^2} \frac{\operatorname{sgn}\left(i_{my}\right)}{\left(e^{\frac{i_Y}{2}}+e^{-\frac{i_Y}{2}}\right)^2} \end{aligned} \quad (4)$$

The analysis of (4) further shows that, independently from the numerical values of the parameters, the signs requirements described in [38] are satisfied. Finally, the self-saturation dynamic inductances on the direct and quadrature axis can be defined as:

$$\begin{aligned} L'_{sx} = \frac{d\Psi_{sx}}{di_{mx}} &= \eta_1 + 2\alpha_1\beta_1 + \frac{1}{\left(e^{\frac{\beta_1 i_{mx}}{2}}+e^{-\frac{\beta_1 i_{mx}}{2}}\right)^2} + \\ &+ \frac{\gamma}{\sigma_1^2} \frac{e^{\frac{i_X}{2}}-e^{-\frac{i_X}{2}}}{\left(e^{\frac{i_X}{2}}+e^{-\frac{i_X}{2}}\right)^3} \frac{1}{1+e^{-i_Y}} \end{aligned} \quad (5)$$

$$\begin{aligned} L'_{sy} = \frac{d\Psi_{sy}}{di_{my}} &= \eta_2 + 2\alpha_2\beta_2 + \frac{1}{\left(e^{\frac{\beta_2 i_{my}}{2}}+e^{-\frac{\beta_2 i_{my}}{2}}\right)^2} + \\ &+ \frac{\gamma}{\sigma_2^2} \frac{e^{\frac{i_Y}{2}}-e^{-\frac{i_Y}{2}}}{\left(e^{\frac{i_Y}{2}}+e^{-\frac{i_Y}{2}}\right)^3} \frac{1}{1+e^{-i_X}} \end{aligned} \quad (6)$$

As for the static inductances, they are straightforwardly defined as:

$$\begin{aligned} L_{sx} = \frac{\Psi_{sx}}{i_{mx}} &= 2\alpha_1 \frac{1}{i_{mx}} \left(\frac{1}{1+e^{-\beta_1 i_{mx}}} - \frac{1}{2}\right) + \eta_1 + \\ &- \frac{\gamma}{\sigma_1} \frac{1}{i_{mx}} \frac{\operatorname{sgn}\left(i_{mx}\right)}{\left(e^{\frac{i_X}{2}}+e^{-\frac{i_X}{2}}\right)^2} \frac{1}{1+e^{-i_Y}} \end{aligned} \quad (7)$$

$$\begin{aligned} L_{sy} = \frac{\Psi_{sy}}{i_{my}} &= 2\alpha_2 \frac{1}{i_{my}} \left(\frac{1}{1+e^{-\beta_2 i_{my}}} - \frac{1}{2}\right) + \eta_2 + \\ &- \frac{\gamma}{\sigma_2} \frac{1}{i_{my}} \frac{\operatorname{sgn}\left(i_{my}\right)}{\left(e^{\frac{i_Y}{2}}+e^{-\frac{i_Y}{2}}\right)^2} \frac{1}{1+e^{-i_X}} \end{aligned} \quad (8)$$

The analysis of the vector electric circuit in Fig. 2 shows that, if the iron losses are taken into consideration, the stator current is not a state variable anymore. The state variable is, under this assumption, the magnetizing current vector.

B. State Formulation of the Dynamic Model

Considering the voltage equation and the Kirchhoff current equation in the node, the motor equations can be written as a function of the stator flux space vector $\mathbf{\Psi}_s$:

$$\frac{d\mathbf{\Psi}_s}{dt} = -\left(\frac{R_s R_0}{R_s+R_0}\mathbf{L}_s^{-1} + jp\omega_r\right)\mathbf{\Psi}_s + \frac{R_0}{R_s+R_0}\mathbf{u}_s \quad (9)$$

If the magnetizing current $\mathbf{i}_m$ is chosen as state variable, then, after some manipulations with the matrix algebra, the following matrix equations can be written:

$$\frac{d\mathbf{i}_{mx}}{dt} = \mathbf{L}_s'^{-1}\left(-\left(\frac{R_s R_0}{R_s+R_0} + \mathbf{J}\omega_r\mathbf{L}_s\right)\mathbf{i}_m + \frac{R_0}{R_s+R_0}\mathbf{u}_s\right) \quad (10a)$$

$$\mathbf{i}_s = \frac{R_0}{R_s+R_0}\mathbf{i}_m + \frac{1}{R_s+R_0}\mathbf{u}_s \quad (10b)$$

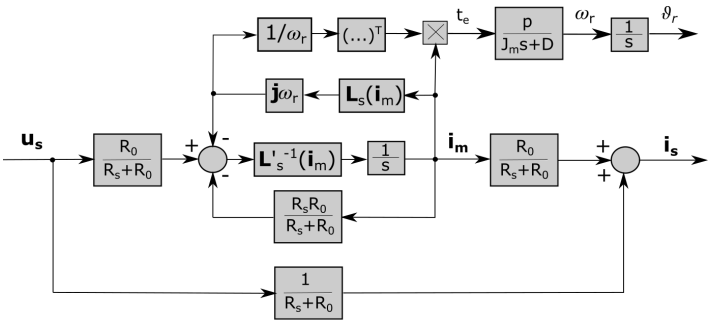

Fig. 3: Block diagram of the SynRM including iron losses

(10) represent the state representation of the space-vector model of the SynRM, assuming the magnetizing current as state variable, in the form:

$$\frac{d\mathbf{x}}{dt} = \mathbf{A}\mathbf{x} + \mathbf{B}\mathbf{u}$$
$$\mathbf{y} = \mathbf{C}\mathbf{x} + \mathbf{D}\mathbf{u}$$

where $\mathbf{x}$ is the state vector, $\mathbf{u}$ is the input vector, $\mathbf{y}$ is the output vector and the remaining matrices are:

$$\begin{aligned}
\mathbf{A} &= -\mathbf{L}_s'^{-1}\left(\frac{R_s R_0}{R_s+R_0} + \mathbf{J}\omega_r \mathbf{L}_s\right)\\
\mathbf{B} &= \mathbf{L}_s'^{-1}\frac{R_0}{R_s+R_0}\\
\mathbf{C} &= \frac{R_0}{R_s+R_0}\\
\mathbf{D} &= \frac{1}{R_s+R_0}
\end{aligned} \tag{11}$$

where:

$$\mathbf{L}_s'^{-1} = \frac{1}{L'_{sx}L'_{sy} - L'^{2}_{sxy}}\begin{bmatrix} L'_{sy} & -L'_{sxy} \\ -L'_{sxy} & L'_{sx} \end{bmatrix} \tag{12}$$

The analysis of (10) highlights that the magnetizing current is the state of the system, and depends on the stator voltage. The output of the system, that is the stator current vector, is a linear combination of the magnetizing current (state) and stator voltage (input). If R_0 tends to infinite, $\mathbf{i}_s = \mathbf{i}_m$ and (10 a) coincides with the model in [21]. Fig. 3 shows the block diagram of the proposed dynamic model (10).

C. Derivation of the Electromagnetic Torque

The expression of the electromagnetic torque can be found starting from the input-output instantaneous power balance:

$$P = \frac{3}{2}\mathbf{u}_s^T \mathbf{i}_s.$$

Exploiting the voltage equation of the electric circuit in Fig. 2, the instantaneous active power becomes:

$$P = \frac{3}{2}R_s \mathbf{i}_s^T \mathbf{i}_s + \frac{3}{2}\left(\mathbf{J}\omega_r \mathbf{L}_s \mathbf{i}_m\right)^T \mathbf{i}_s + \frac{3}{2}\left(\mathbf{L}_s'\frac{d\mathbf{i}_m}{dt}\right)^T \mathbf{i}_s \tag{13}$$

Given that $\mathbf{i}_s = \mathbf{i}_m + \mathbf{i}_0$, it follows:

$$P = \underbrace{\frac{3}{2}R_s \mathbf{i}_s^T \mathbf{i}_s}_{\text{ohmic losses}} + \underbrace{\frac{3}{2}\left(\mathbf{J}\omega_r \mathbf{L}_s \mathbf{i}_m\right)^T \mathbf{i}_m}_{\text{mech. power}} + \\ + \underbrace{\frac{3}{2}\left(\mathbf{J}\omega_r \mathbf{L}_s \mathbf{i}_m\right)^T \mathbf{i}_0}_{\text{iron losses}} + \underbrace{\frac{3}{2}\left(\mathbf{L}_s'\frac{d\mathbf{i}_m}{dt}\right)^T \mathbf{i}_0}_{\text{trans. iron losses}} \tag{14}$$

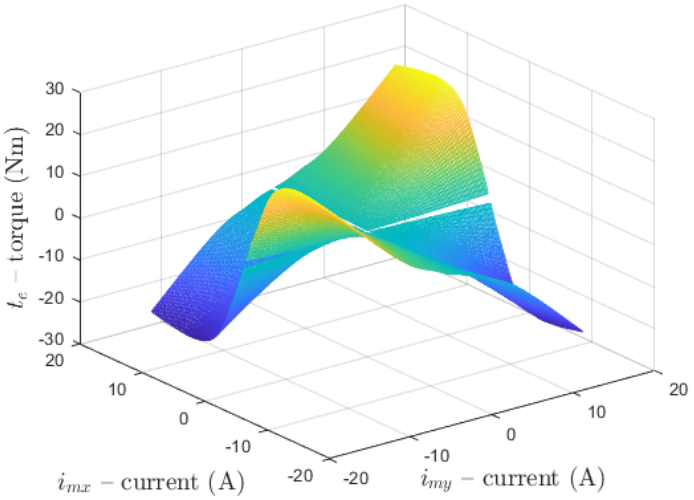

Fig. 4: Electromagnetic torque produced by the SynRM as a function of the state i_m

since:

$$\frac{3}{2}\left(\mathbf{L}_s'\frac{d\mathbf{i}_m}{dt}\right)^T \mathbf{i}_m = 0$$

Eq. (14) states that the instantaneous input power is balanced by the stator ohmic losses, by the iron losses, by the transient iron losses and finally by the produced output mechanical power. The net electromagnetic torque produced by the SynRM can be finally found as a function of the state i_m:

$$t_e = 3/2\left[\mathbf{J}\mathbf{L}_s \mathbf{i}_m\right]^T \mathbf{i}_m = 3/2(L_{sx} - L_{sy}) i_{mx} i_{my} \tag{15}$$

It can be noted that the net electromagnetic torque depends on the vector product between the stator flux and the magnetizing current, the angle between the two depends only on the saliency ratio of the machine. The torque reduction caused by the iron losses can be finally found as a function of the state i_m:

$$\begin{aligned} t_{Fe} &= \frac{3}{2}\left[\mathbf{J}\mathbf{L}_s \mathbf{i}_m\right]^T \mathbf{i}_0 = \frac{3}{2}\frac{\omega_r}{R_0}\left[\mathbf{J}\mathbf{L}_s \mathbf{i}_m\right]^T \mathbf{J}\mathbf{L}_s \mathbf{i}_m = \\ &= \frac{3}{2}\frac{\omega_r}{R_0}\left(L_{sx}^2 i_{mx}^2 + L_{sy}^2 i_{my}^2\right) \end{aligned} \tag{16}$$

It can be noted that the torque reduction increases for decreasing values of R_0, as expected; if R_0 tends to infinity, the torque loss due to the iron losses tends to zero. The torque loss is also proportional to the supply frequency and the square of the flux (and correspondingly to the square of the magnetizing current), coherently with the well-known Steinmetz expression.

Fig. 4 shows the surface describing the electromagnetic torque t_e as a function of the direct and quadrature components of the magnetizing current i_{mx}, i_{my}, obtained based on (15), where the static inductances L_{sx}, L_{sy} are themselves functions of the magnetizing current components according to (7), (8) (see Fig.s 16, 17). The surface is related to the SynRM under test, whose rated data are given in Tab. I, and whose magnetic model parameters have been experimentally identified according to the method in [20] and shown in Tab. II. It can be observed that the surface is highly nonlinear, first because it depends on the product of the two components of the magnetizing current, and second because it depends also on the product of the static inductances, both non-linearly variable with the magnetizing current components. The

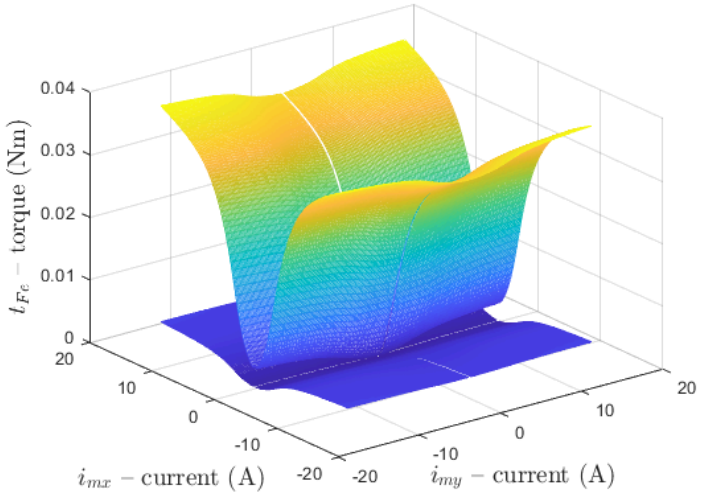

Fig. 5: Torque reduction caused by the iron losses as a function of the state i_m

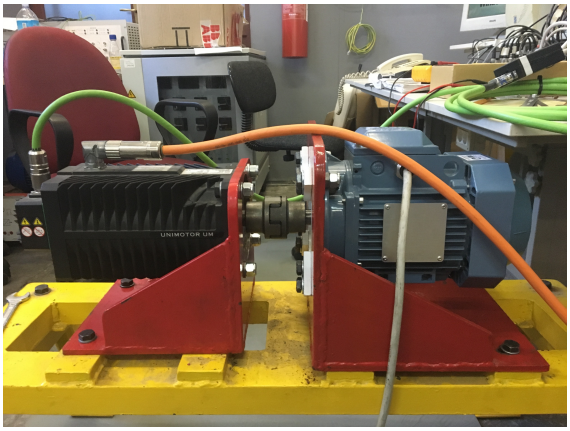

Fig. 6: Photograph of the Experimental Set-up

electromagnetic torque increases with the increase of both i_{mx}, i_{my}, being positive when they present the same sign. In particular, while the variation of t_e with i_{my} does not present saturation effects, according to the poorly saturable magnetic circuit on the quadrature axis, the variation of t_e with i_{mx} present a remarkable saturation effect, coherently with the highly saturable magnetic circuit on the direct axis. Fig. 5 shows the surface describing the loss of torque caused by the iron losses versus the direct and quadrature components of the magnetizing current i_{mx}, i_{my}, obtained based on (16). Since the loss of torque caused by the iron losses depends also on the motor speed, the surface has been plotted for 2 values of motor speed, respectively 20 rad/s and 100 rad/s. It can be observed that the loss of torque has always the same sign, independently from the signs of i_{mx}, i_{my} and it increases with both of them, as expected. It increases, however, strongly with i_{mx} and far less with i_{my}, due to the dependence on the square of the static inductances ($L_{sy} \ll L_{sx}$). Finally, the higher the motor speed is, the higher the loss of torque is, as expected. The surfaces in Fig.s 4 and 5 have been obtained after the parametrization of the SynRM under test, shown in Fig. 6.

TABLE I: Rated data of the *SynRM*

rated power (kW)	2.2
rated voltage (V)	380
rated frequency (Hz)	50
pole-pairs	2
rated speed (rpm)	1500
rated current $(ARMS)$	5.5
rated torque (Nm)	14

TABLE II: Identified model parameters

model parameter	value
α_1	1.2139
β_1	0.4848
η_1	0.0111
α_2	0.3609
β_2	0.4033
η_2	0.0042
γ	0.1565
μ_1	2.1612
σ_1	0.6221
μ_2	3.3430
σ_2	0.9706
R_0	1330

D. Comparison with other analytical magnetic models

The proposed magnetic model is in the framework of the flux vs current approaches. It represents an evolution of a previous contribution of the authors [22], with which it shares the physical underlying analysis. All the comparative considerations related to [22] are therefore valid also regarding the approach proposed in this paper. Besides the contributions [16]–[19], already cited in the introduction, a specific comment should be made on the approach presented in [13], that is the most recent and one of the most complete approaches. [13] focuses on the magnetic modelization of both IPMSMs and SynRMs. It specifically proposes physically motivated analytical non-linear flux versus current functions that permit consideration of both self and cross-saturation. As for the self-saturation phenomenon, it proposes a combination of the $\tanh(\cdot)$ and a linear function. From this point of view, the approach in [13] is the same already proposed by the authors in [22]. As for the cross-saturation phenomenon, the approach in [13] is only slightly different from that proposed by the authors in [22]. Both these approaches respect the reciprocity conditions. In detail, the underlying physical conditions exploited for the definition of the covariance energy variation function are the same. The first difference lies in the function describing the variation of the flux with the stator current component on the same axis for a given value of current on the other axis ($\Psi_{sx} = f(i_{sx}, i_{sy})|_{i_{sy}=k}$): compare (19) and (20) in [13] with second terms of (5) in [22]. In [13] the adopted function is based on the difference between two $\tanh(\cdot)$ and linear functions, both centered at zero current. In [22] the adopted function is a $1/\cosh(\cdot)$ centered on a predetermined value of current. Such two waveforms both present a bell-like shape, the first one asymmetric, the second symmetric. Both functions, if properly parametrized, can represent the same kind of data. As for the function describing the variation of the flux with the stator current component on the other axis for a given current value on the same axis ($\Psi_{sx} = f(i_{sx}, i_{sy})|_{i_{sx}=k}$), there are major differences between the approaches in [13] and [22]. [13] proposes a quadratic and a $\log(\cosh(\cdot))$ function, centered at zero current, while [22] proposes a $\tanh(\cdot)$ function, centered at a predefined value of the current and weighted with a $\mathrm{sgn}(\cdot)$

function to account for the same variation of the flux with different signs of the load. The main difference between the two approaches is that, while [13] considers an unlimited reduction of the flux with the load current, [22] considers a saturation of such effect above certain values of the load current (due to the $\tanh(\cdot)$). The approach proposed in this paper is based on a combination of exponential functions, presenting the same kind of waveforms of [22]. From this point of view, as cited above, the considerations written about the approach in [22] are valid also for the approach proposed here. [13] proposes also a second function describing the cross-saturation effect. Such an approach is based on the combination of exponentials of the type $1-e^{(\cdot)^2}$. Such an approach presents a saturation phenomenon of the flux variation with the load current, that is analogous to that proposed by the authors in [22], and therefore to the approach proposed here. The approach adopted in [13] for the analytical representation of the magnetic model is just slightly different from that in [22] and that in the proposed paper. In general, however, the proposed approach improves [13] in the fact that it proposes a state representation of the model, useful for control purposes, as well as in the fact that it includes iron losses.

III. Identification of iron losses resistance R_0

Among the off-line measurement/estimation techniques of the iron losses resistance, the approaches in [31], [33], [34] have to be cited. [33] proposes a classic measurement method of the iron losses resistance requiring precise measurement of the mechanical losses of the drive system. [34] shows the results of an off-line measurement of the iron losses resistance, but it does not describe the adopted methodology. The methodology proposed in this paper is inspired by that in [31], improving it in the fact that it does not require the recognition of the condition of zero torque (difficult to be measured), while it is based on the recognition of the orthogonality condition between the back emf and the stator current space vectors. [32], on the contrary, proposed a numerical method for estimating off-line the iron losses based on FEA (Finite Element Analysis).

A specific methodology has been devised for identifying the resistance R_0 (see Fig. 2) responsible for the iron losses of the SynRM, as well as its variation with the motor speed ω ($p\omega = \omega_r$ the supply frequency) and stator flux amplitude $|\mathbf{\Psi}_s|$. To this aim, the PMSM drive mechanically coupled to the SynRM (see Sec. V) has been suitably exploited. In particular, the speed of the PMSM drive has been closed-loop controlled adopting a classic field-oriented control (FOC) technique. As the typical hierarchy of the nested control loops of electric drives, a torque loop is present inside the speed one, whose reference is the output of the speed controller. The actual torque produced by the PMSM is therefore a measured quantity of the system. Given a constant speed reference to the PMSM drive, the stator current of the SynRM drive has been closed-loop controlled in the rotor reference frame. A constant current reference on the direct (x) axis has been given to the drive, with the direct (x) axis initially lying in the direction of minimum reluctance. Once the current has tracked its set-point, the synchronous reference frame adopted for current control ($x-y$) has been rotated by a certain angle $\Delta\theta$ so that stator current space-vector becomes orthogonal to the motor back emf space vector $\mathbf{e}_s$. To this aim, the angle of the back emf $\mathbf{e}_s$ with respect to the axis of minimum reluctance x has been previously detected. This condition ensures that, in this

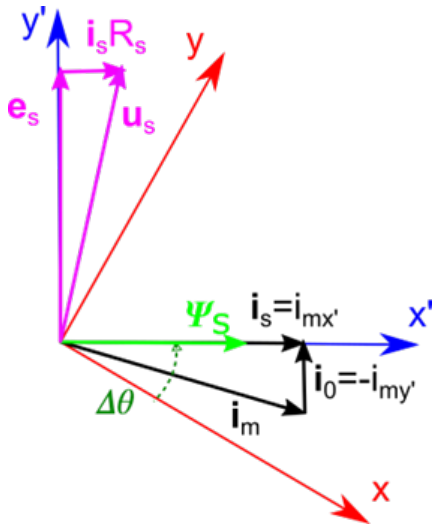

Fig. 7: Space-vector diagram of the system for measuring R_0

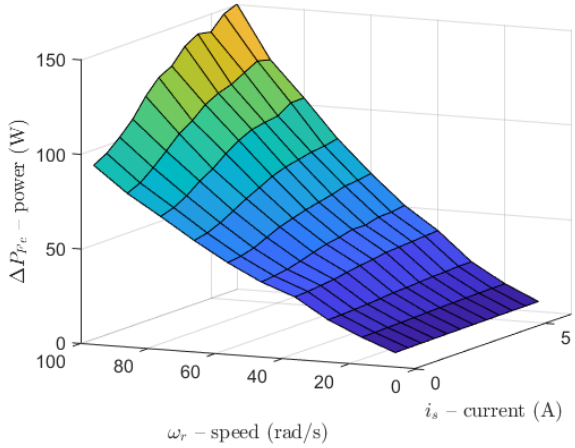

Fig. 8: Iron losses versus speed and stator current amplitude surface

new reference frame ($x'-y'$), the stator flux space vector $\mathbf{\Psi}_s$ lies in the direction of the stator current $\mathbf{i}_s$, being $\mathbf{\Psi}_s$ orthogonal to $\mathbf{e}_s$. Since the iron losses current $\mathbf{i}_0$ is in phase with $\mathbf{e}_s$, it implies that $\mathbf{i}_s = i_{mx'}$ and $\mathbf{i}_0 = -i_{my'}$. The corresponding space-vector diagram describing this working condition is sketched in Fig. 7. In these working conditions, the quadrature magnetization current $i_{my'}$ assuming a negative value, exactly compensate for the iron losses current $\mathbf{i}_0$ thus generating a net resistant torque equal to the loss of torque caused by the iron losses. In such working conditions, the SynRM absorbs active power only for compensating the stator joule losses. The PMSM drive, on the contrary, must generate a torque compensating for the mechanical friction and the iron losses torques.

Starting from the above considerations, a complete mapping of the system has been made. The speed of the SynRM has been modified, step by step in a wide range, acting on the PMSM drive speed reference. At each speed value, the amplitude of the SynRM stator current has been modified in a wide range according to the above-described procedure. At each working point, the mechanical friction losses ΔP_{fr} have been measured as the product between the torque and speed of the PMSM drive, under the conditions in which the SynRM is not supplied.

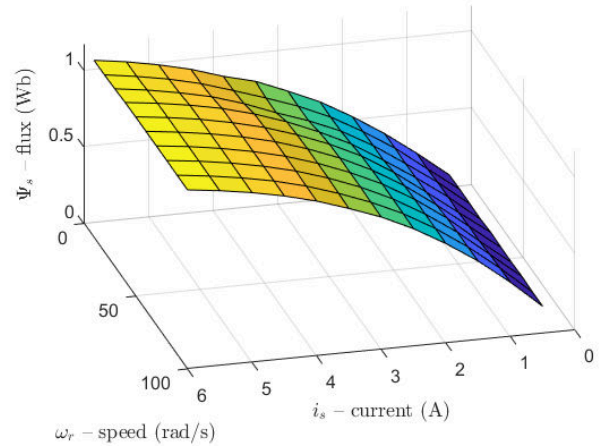

Fig. 9: Stator flux amplitude versus speed and stator current amplitude surface

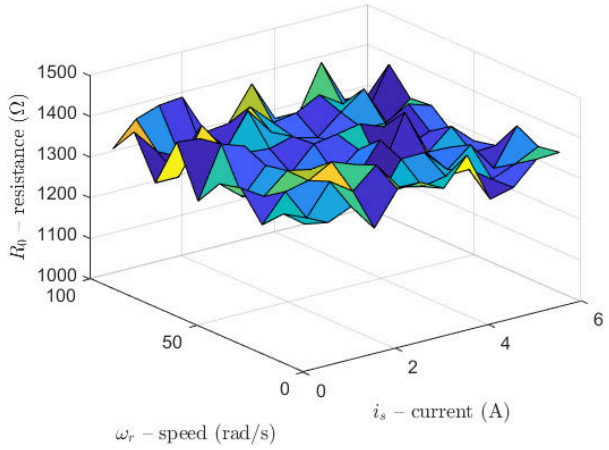

Fig. 10: Iron losses resistance versus speed and stator current amplitude surface

Analogously, the sum between the mechanical friction losses and the iron losses $\Delta P_{meas} = \Delta P_{fr} + \Delta P_{Fe}$ have been measured as the product between the torque and speed of the PMSM drive, under the conditions in which the SynRM is supplied as above described. Fig. 11 shows the scheme adopted for the measurement of the iron losses resistance R_0, where the control actions on the PMSM and SynRM drives are highlighted. The iron losses have been obtained as the difference between the last two. Fig. 8 shows the iron losses versus speed and stator current amplitude

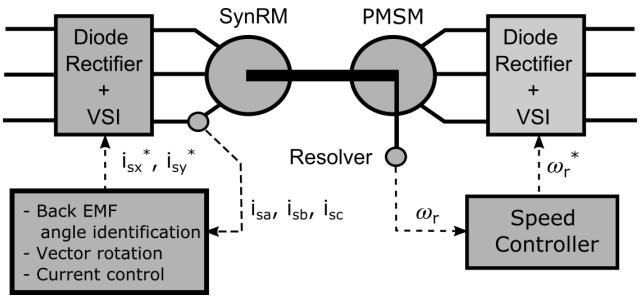

Fig. 11: Scheme adopted for the measurement of R0

surface, as experimentally obtained on the test set-up described in Sec. V. As a final result of this identification process, Fig. 9 shows the corresponding stator flux amplitude versus speed and stator current amplitude surface. In this case, the stator flux amplitude has been measured as:

$$|\mathbf{\Psi}_s| = \frac{|\mathbf{e}_s|}{\omega_r} = \frac{|\mathbf{u}_s - R_s \mathbf{i}_s|}{\omega_r}$$

so the measurement does not suffer from any error in the knowledge of the magnetic characteristic of the machine. Finally, Fig. 10 shows the corresponding iron losses resistance versus speed and stator current amplitude surface, obtained as:

$$R_0 = \frac{3}{2}\frac{|\mathbf{e}_s|^2}{\Delta P_{Fe}}$$

It can be observed that the iron losses increase with the speed almost with a quadratic law, while it increases less than quadratically with the current. This is due to the saturation of the iron core for increasing values of the stator current amplitude. This is confirmed by the stator flux amplitude surface. On the contrary, the R_0 surface shows, for the SynRM under test, a very limited variation with both the speed and the stator current amplitude, that justifies the assumption of constant value of R_0 in Fig. 2.

IV. Effect of Magnetic Saturation and Iron Losses on MTPA and MTPV Techniques

As for the specific effect of magnetic saturation on the MTPA, the authors have proposed an analytical formulation of the MTPA considering magnetic saturation in [40]. This technique exploits a simplified magnetic model to retrieve an analytical formulation of the MTPA. In [40] is clearly shown that, because of the effect of the magnetic saturation, the function relating the direct and quadrature stator current references ($i_{sx,ref} = f(i_{sy,ref})$) presents a saturation.

As for the specific effect of iron losses on the MTPA, to the best of the authors' knowledge, the scientific literature does not present many contributions. In particular, [34] shows that if iron losses have to be accounted for in the formulation of the MTPA, the reference value of the direct component of the stator current must be slightly increased for a given value of the load torque (or for a given value of the stator current amplitude), as visible in Fig.s 6 and 7 from [34]. This result is confirmed also in the master thesis [41] from Politecnico di Torino, Italy (see Fig.s 3.13a and 13b in [41]) and by [35] showing that the stator current angle reference increases because of the presence of the iron losses (see (9) in [35]). This effect is to be expected, given that the iron losses cause a slight decrease of the generable electromagnetic torque.

As for the specific effect of the saturation and iron losses on the MTPV, [42] stresses clearly that the voltage angle command of MTPV is fixed at 45° and that if the drive is operated out of this 45° boundary, the control system becomes unstable because the pull-out torque condition is reached. It stresses also that although saturation has a strong effect on the MTPA of SynRM, it does not have a significant effect on the MTPV. In [42] there is no analysis of the effect of iron losses on MTPV operation. [43] treats the MTPV from the point of view of the current angle command, and shows the constant current angle to be maintained in MTPV depending on the ratio between the direct and quadrature inductance, assumed constant (see (1) in [43]).

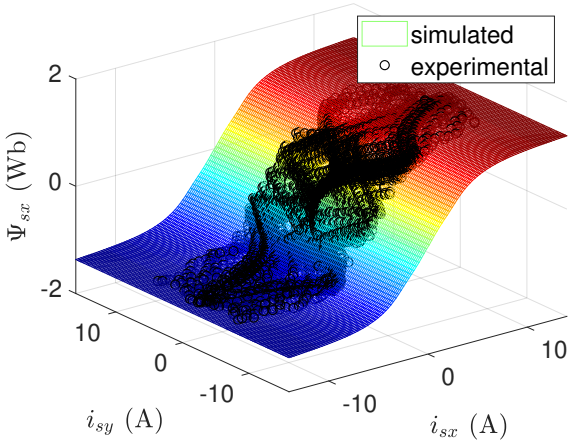

Fig. 12: $\Psi_{sx} = f_1(i_{sx}, i_{sy})$

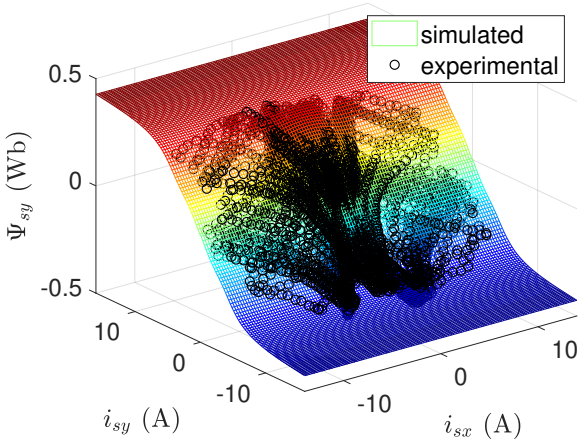

Fig. 13: $\Psi_{sy} = f_2(i_{sx}, i_{sy})$

The effect of magnetic saturation on the MTPV current angle is shown based on FEA analysis. Also in [42] there is no analysis of the effect of iron losses on MTPV operation. In [30] it is explicitly emphasized that the field-weakening range is decreased by saturation and iron-loss effects.

V. Experimental Setup

The proposed model has been validated experimentally by adopting a suitably developed test set-up with the SynRM motor model ABB 3GAL092543-BSB, whose rated values are shown in Tab. I. The SynRM is mechanically coupled to a torque-controlled permanent magnet synchronous motor (PMSM) drive working as an active load. The SynRM is supplied by a Voltage Source Inverter (VSI) with insulated gate bipolar transistor (IGBT) modules, model Semikron SMK 50 GB 123, driven by a space-vector Pulse Width Modulation technique (SV-PWM) with PWM frequency set to 5 kHz. Fig. 6 shows the photo of the SynRM drive test set-up.

VI. Experimental Validation of the Proposed Model

A. Parameters estimation of the magnetic model

As for the estimation of the set of parameters of the magnetic model in Sec. II-B, the methodology adopted in [20] has been exploited here: it is based on three standstill tests. The readers can refer to [20] for a specific description of the identification technique. Tab. II summarises the final values of the parameters, as obtained at the end of the identification process. The methodology is based on the minimization of the flux error. The obtained final value of the mean square error obtained at the end of the identification process is 0.034 Wb, (on a rated flux of 1 Wb).

As a final result of the overall identification process, including both the self and cross-saturation characterizations, Fig.s 12 and 13 show the surfaces describing the functions $\Psi_{sx} = f_1(i_{mx}, i_{my})$, and $\Psi_{sy} = f_2(i_{mx}, i_{my})$, respectively the experimental measurements (black circles) and the surfaces describing the interpolating functions in (1). It can be observed that the interpolating functions well match the experimental points, witnessing the correctness of the identification process.

As for the self-inductances, Fig.s 14, 15, 16, and 15 show respectively the dynamic self-inductance surfaces $L'_{sx} = h_1(i_{mx}, i_{my})$, and $L'_{sy} = h_2(i_{mx}, i_{my})$ as well as the static

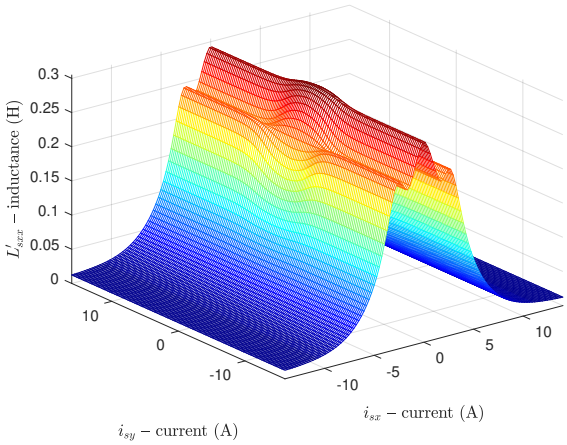

Fig. 14: Self-saturation inductance L'_{sx} vs i_{mx}, i_{my}

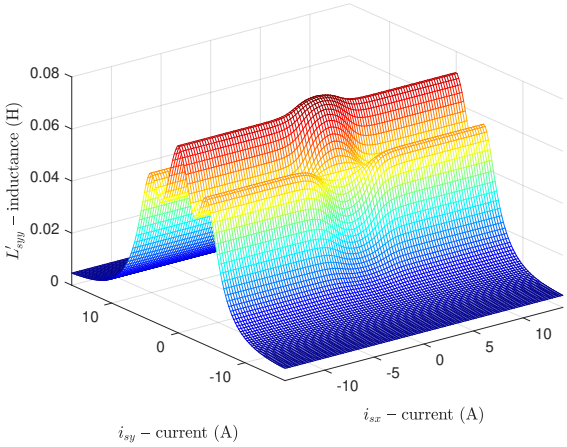

Fig. 15: Self-saturation inductance L'_{sy} vs i_{mx}, i_{my}

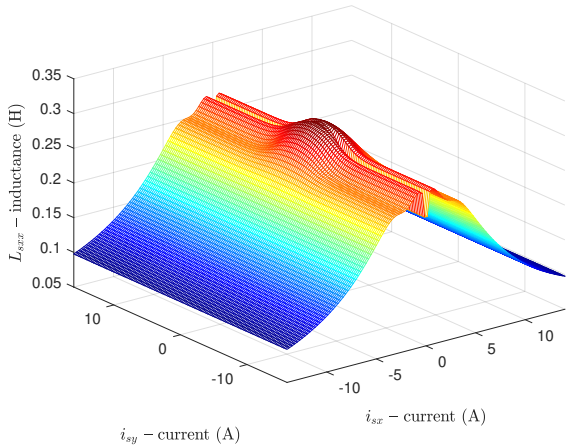

Fig. 16: Cross-saturation inductance L_{sx} vs i_{mx}, i_{my}

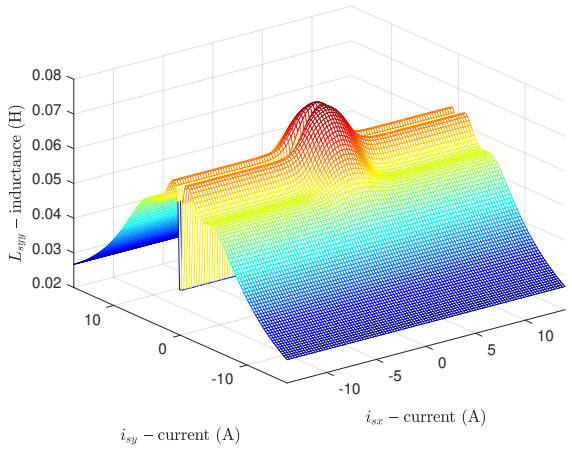

Fig. 17: Self-saturation inductance L_{sy} vs i_{mx}, i_{my}

self-inductance surfaces $L_{sx} = g_1(i_{mx}, i_{my})$, and $L_{sy} = g_2(i_{mx}, i_{my})$. Such surfaces describe respectively, the interpolating functions in (5)-(6) and in (7)-(8).

As for the dynamic self-inductances, such figures clearly show that L'_{sx} varies mainly with i_{mx}, while it is only moderately influenced by i_{my}, as expected. In particular, L'_{sx} decreases with i_{mx} as soon as magnetic saturation occurs. The effect of i_{my} on L'_{sx} is more visible for lower values of i_{mx}, when the machine is not still fully saturated, while it becomes hardly observable as soon as the machine is fully saturated. The higher the value of i_{my} (in absolute terms), the higher such effect is confirming the reduction of the dynamic self-inductance for increasing values of the load. Above some values of i_{mx}, the magnetic circuit is already so saturated that the load has a minimum impact, independently of the amplitude of i_{my} . L'_{sy} presents a shape similar to that of L'_{sx}, excepted that it presents a more observable dependence on i_{mx}. The same considerations could be made for the static self-inductances, which present a shape similar to that of the dynamic inductances, being slightly smoother.

As for the cross-saturation phenomenon, Fig.s 18, 19 and 20 show the surfaces of respectively the co-energy variation $\Delta W' = g_c(i_{mx}, i_{my})$ representing (2), the flux variation caused by the cross-saturation on the x-axis $\Delta\Psi_{sx} = \Delta f_1(i_{mx}, i_{my})$ representing the second part of (1), and the cross-saturation

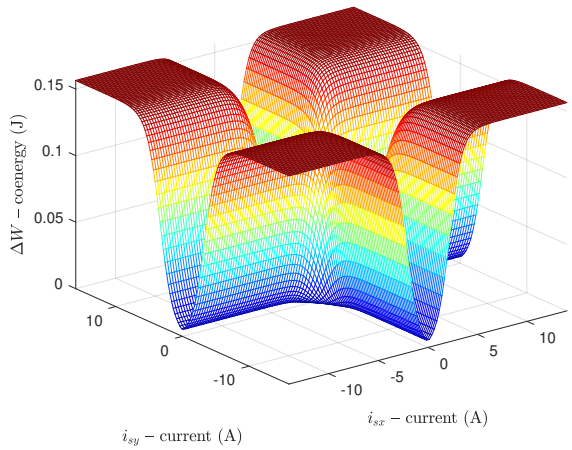

Fig. 18: Co-energy variation $\Delta W'$ vs i_{mx}, i_{my}

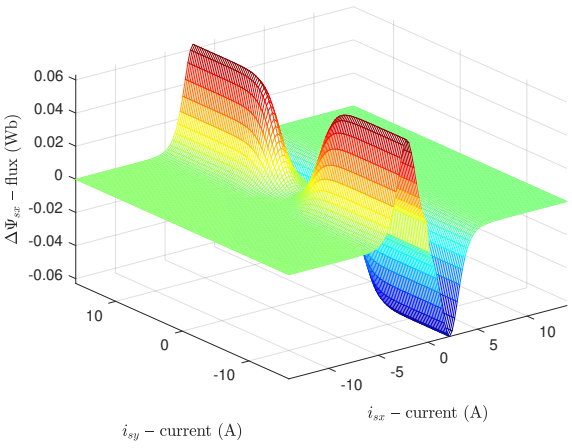

Fig. 19: $\Delta\Psi_{sx} = \Delta f_1(i_{mx}, i_{my})$ due to the cross-saturation

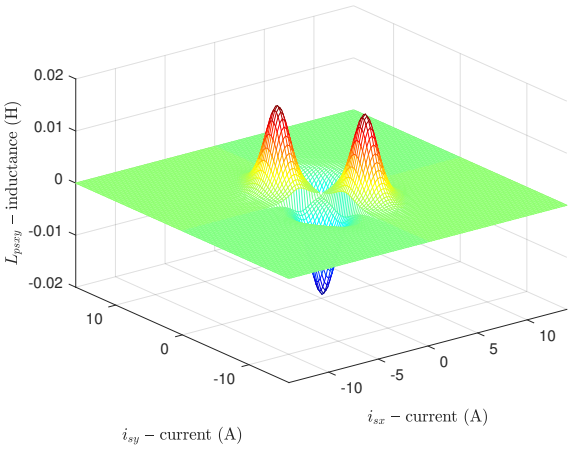

Fig. 20: Cross-saturation inductance L'_{sxy} vs i_{mx}, i_{my}

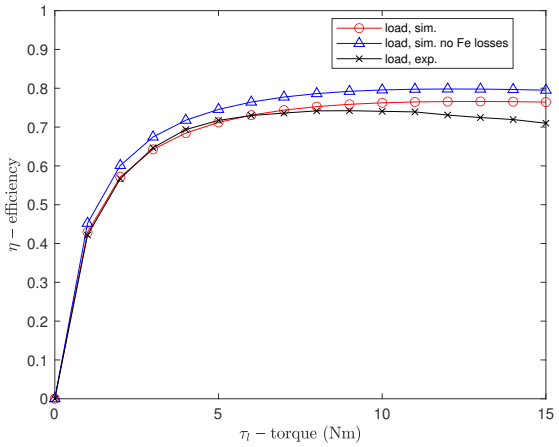

Fig. 21: Percent efficiency η vs load torque T_l

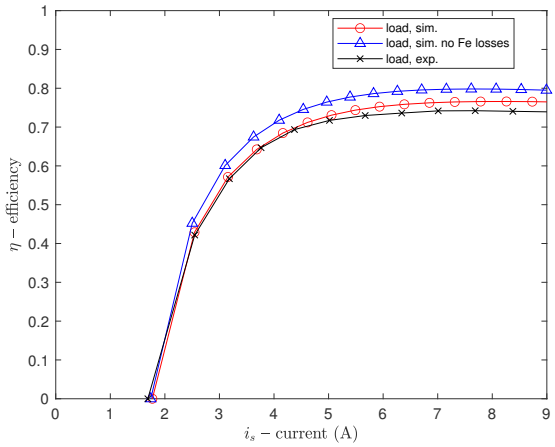

Fig. 22: Percent efficiency η vs current vector amplitude $|\mathbf{i}_s|$

dynamic inductance $L'_{sxy} = f_c(i_{mx}, i_{my})$ representing (4), as obtained at the end of the identification process. The co-energy variation surface presents a null value for null values of both i_{mx}, i_{my}, and increases in amplitude maintaining a positive sign as soon as any current increases in absolute terms, as expected given the physical meaning of this variable. The flux variation on the x-axis due to the cross-saturation firstly increases with i_{mx}, and then decreases with it, following the sign of i_{mx}. On the contrary, it always increases with i_{my} (load), maintaining the same sign independently from the sign of i_{my}, as expected based on the physics of the phenomenon. As for the dynamic cross-inductance, it can be noted that there are specific current ranges in which it is non-null, with maxima values obtained for specific values of i_{mx}, i_{my} while elsewhere it is close to zero because of the full saturation of the magnetic circuit. Additionally, the cross-saturation dynamic inductance presents a negative sign when the current components present equal signs, while it presents a positive sign when the current components present opposite signs, according to the analysis in [38].

B. Experimental validation

To experimentally validate the proposed model, since iron losses play a role in the overall machine losses, the steady-state percent efficiency has been chosen as the variable to be investigated. To this aim, the efficiency of the SynRM under test has been measured, according to the variation of the load and the speed. The efficiency has been measured directly: the output power has been measured as the product between the load torque (well known since it is the command provided to the industrial torque-controlled PMSM drive working as active load) and measured speed. The input active power has been measured based on the reference values of the stator voltages and the stator currents, according to $P = 3/2\mathbf{u}_s^T\mathbf{i}_s$. The SynRM drive has been controlled with a classic rotor-oriented control (ROC) and operated under the MTPA strategy developed in [40]. The experimental measurements have been then compared with the corresponding simulation results obtained in 2 different scenarios: 1) the proposed model (considering both magnetic saturation and iron losses), 2) the model considering only magnetic saturation while neglecting iron losses [22].

Fig. 21 shows the percent efficiency versus the load torque, obtained for a constant working speed of $100\,rad/s$. It can be

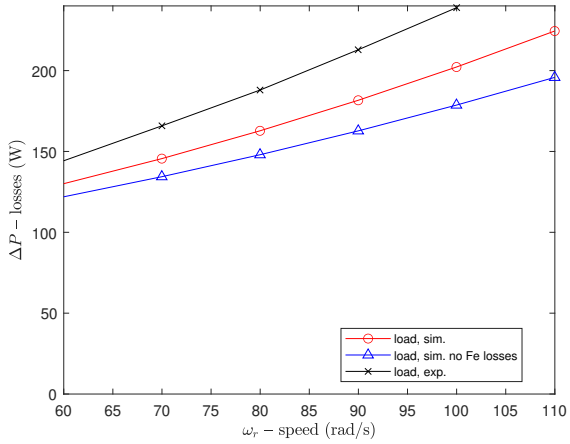

Fig. 23: Total losses ΔP vs rotating speed ω_r

observed that the efficiency increases with the load in a wide load range, as expected, being null for the null load torque. Above the load torque of about $9\,Nm$, the efficiency starts slightly decreasing. It can be noted that the efficiency curve simulated with the proposed model, accounting also for the iron losses, better matches the experimental one with respect to the model not accounting for the iron losses [22], as expected. In particular, the proposed model very well estimates the efficiency for low and medium loads, while small estimation errors occur at very high loads, due to physical phenomena not accounted for by the model (space harmonics of the mmf combined with time harmonics of the voltage supply etc.). Fig. 22 shows the percent efficiency versus the amplitude of the stator current space-vector, obtained for a constant working speed of $100\,rad/s$. It can be observed that the shape of such a curve is analogous to the efficiency vs load curve. It presents a null value for a nonnull value of the stator current (no load condition with the machine magnetized). Even in this case, the efficiency curve simulated with the proposed model, accounting also for the iron losses, better matches the experimental one with respect to the model not accounting for them [22]. Finally, Fig. 23 shows the overall electric losses of the SynRM versus its speed, obtained for a constant stator current amplitude of $5\,A$. This figure shows that, for a given stator current amplitude (given joule losses), the overall electric losses increase

with the rotor speed with almost quadratic law. This is to be expected, being the iron losses responsible for the variation of the electric losses with the speed, and varying themselves with the supply frequency with almost quadratic law. Conforming to the efficiency results, the curve simulated with the proposed model, accounting also for the iron losses, better matches the experimental one with respect to the model not accounting for the iron losses [22], as expected. All the above results permit to properly validate the proposed model and highlight its higher accuracy in describing the energetic behavior of the SynRM.

VII. Conclusions

This paper proposes a space-vector dynamic model of the Synchronous Reluctance Motor (SynRM) including both self-saturation, cross-saturation effects, and iron losses expressed in state form, where the magnetizing current has been selected as a state variable. The proposed dynamic model is based on an original function between the stator flux and the magnetizing current components, improving a previously developed magnetic model. It is noteworthy that the proposed model includes not only magnetic saturation but also iron losses. The static and dynamic inductance expressions have been analytically developed so that the reciprocity condition for the cross-saturation can be satisfied. A suitably developed identification technique has been employed for the estimation of the parameters of the magnetic model, including the resistance describing the iron losses. The proposed parameter estimation technique has been successfully assessed in numerical simulations as well as experimentally on a suitably developed test set-up.

References

[1] A. Accetta, M. Cirrincione, M. Pucci, and A. Sferlazza, "Space-vector State Dynamic Model of the SynRM Considering Self, Cross-Saturation and Iron Losses and Related Identification Technique," *IEEE Transactions on Industry Applications*, vol. 59, no. 3, pp. 3320–3331, May 2023.

[2] N. Bianchi, C. Babetto, and G. Bacco, *Synchronous Reluctance Machines: Analysis, Optimization and Applications*. Institution of Engineering and Technology, Dec. 2021, google-Books-ID: JGJVEAAAQBAJ.

[3] S. A. Nasar, I. Boldea, and L. E. Unnewehr, *Permanent Magnet Reluctance & Self Synchronous Motors*. CRC-Press, Mar. 1993, google-Books-ID: Fd8eAQAAIAAJ.

[4] I. Boldea, *Reluctance Synchronous Machines and Drives*. Clarendon Press, 1996.

[5] J. Faucher, M. Lajoie-Mazenc, and A. Chayegani, "Characterization of a closed-loop controlled current-fed reluctance machine taking into account saturation," *IEEE Transactions on Industry Applications*, vol. IA-15, no. 5, pp. 482–488, Sep. 1979.

[6] A. Fratta and A. Vagati, "A reluctance motor drive for high dynamic performance application," *IEEE Transactions on Industry Applications*, vol. 28, no. 4, pp. 873–879, July 1992.

[7] T. Matsuo and T. A. Lipo, "Field oriented control of synchronous reluctance machine," in *Proceedings of IEEE Power Electronics Specialist Conference - PESC '93*, June 1993, pp. 425–431.

[8] A. Vagati, M. Pastorelli, F. Scapino, and G. Franceschini, "Impact of cross saturation in synchronous reluctance motors of the transverse-laminated type," *IEEE Transactions on Industry Applications*, vol. 36, no. 4, pp. 1039–1046, July 2000.

[9] Y. Li, Z. Q. Zhu, D. Howe, and C. M. Bingham, "Modeling of cross-coupling magnetic saturation in signal-injection-based sensorless control of permanent-magnet brushless ac motors," *IEEE Transactions on Magnetics*, vol. 43, no. 6, pp. 2552–2554, June 2007.

[10] S. Kuehl and R. M. Kennel, "Measuring magnetic characteristics of synchronous machines by applying position estimation techniques," *IEEE Transactions on Industry Applications*, vol. 50, no. 6, pp. 3816–3824, Nov 2014.

[11] S. Kuehl, P. Landsmann, and R. M. Kennel, "Bivariate polynomial approximation of cross-saturated flux curves in synchronous machine models." Florence, Italy: IEEE, 2012, pp. 219–224.

[12] J. Bonifacio and R. M. Kennel, "On Considering Saturation and Cross-Coupling Effects for Copper Loss Minimization on Highly Anisotropic Synchronous Machines," *IEEE Transactions on Industry Applications*, vol. 54, no. 5, pp. 4177–4185, Sep. 2018.

[13] S.-W. Su, C. M. Hackl, and R. Kennel, "Analytical Prototype Functions for Flux Linkage Approximation in Synchronous Machines," *IEEE Open Journal of the Industrial Electronics Society*, vol. 3, pp. 265–282, 2022.

[14] S.-W. Su, H. Börngen, C. M. Hackl, and R. Kennel, "Nonlinear Current Control of Reluctance Synchronous Machines With Analytical Flux Linkage Prototype Functions," *IEEE Open Journal of the Industrial Electronics Society*, vol. 3, pp. 582–593, 2022.

[15] Z. Qu, T. Tuovinen, and M. Hinkkanen, "Inclusion of magnetic saturation in dynamic models of synchronous reluctance motors," in *2012 XXth International Conference on Electrical Machines*, Sep. 2012, pp. 994–1000.

[16] C. Mademlis, "Compensation of magnetic saturation in maximum torque to current vector controlled synchronous reluctance motor drives," *IEEE Transactions on Energy Conversion*, vol. 18, no. 3, pp. 379–385, Sep. 2003.

[17] T. Tuovinen, M. Hinkkanen, and J. Luomi, "Analysis and design of a position observer with resistance adaptation for synchronous reluctance motor drives," *IEEE Transactions on Industry Applications*, vol. 49, no. 1, pp. 66–73, Jan 2013.

[18] A. Kilthau and J. M. Pacas, "Appropriate models for the control of the synchronous reluctance machine," in *Conference Record of the 2002 IEEE Industry Applications Conference. 37th IAS Annual Meeting (Cat. No.02CH37344)*, vol. 4, Oct 2002, pp. 2289–2295.

[19] S. Yamamoto, T. Ara, and K. Matsuse, "A method to calculate transient characteristics of synchronous reluctance motors considering iron loss and cross-magnetic saturation," *IEEE Transactions on Industry Applications*, vol. 43, no. 1, pp. 47–56, Jan 2007.

[20] A. Accetta, M. Cirrincione, M. Pucci, and A. Sferlazza, "A saturation model of the synchronous reluctance motor and its identification by genetic algorithms," in *2018 IEEE Energy Conversion Congress and Exposition (ECCE)*, Sep. 2018, pp. 4460–4465.

[21] ——, "A space-vector state dynamic model of the synchronous reluctance motor including self and cross-saturation effects and its parameters estimation," in *2018 IEEE Energy Conversion Congress and Exposition (ECCE)*, Sep. 2018, pp. 4466–4472.

[22] ——, "Space-vector state dynamic model of synrm considering self- and cross-saturation and related parameter identification," *IET Electric Power Applications*, vol. 14, pp. 2798–2808, December 2020. [Online]. Available: https://digital-library.theiet.org/content/journals/10.1049/iet-epa.2020.0504

[23] H. De Jong, "Saturation in electrical machines," in *Proc. ICEM*, vol. 80, 1980, pp. 1545–1552.

[24] K. A. Corzine, B. T. Kuhn, S. D. Sudhoff, and H. J. Hegner, "An improved method for incorporating magnetic saturation in the q-d synchronous machine model," *IEEE Transactions on Energy Conversion*, vol. 13, no. 3, pp. 270–275, Sep. 1998.

[25] E. Armando, R. I. Bojoi, P. Guglielmi, G. Pellegrino, and M. Pastorelli, "Experimental identification of the magnetic model of synchronous machines," *IEEE Transactions on Industry Applications*, vol. 49, no. 5, pp. 2116–2125, Sep. 2013.

[26] G. Pellegrino, B. Boazzo, and T. M. Jahns, "Magnetic model self-identification for pm synchronous machine drives," *IEEE Transactions on Industry Applications*, vol. 51, no. 3, pp. 2246–2254, May 2015.

[27] S. A. Odhano, P. Giangrande, R. I. Bojoi, and C. Gerada, "Self-commissioning of interior permanent- magnet synchronous motor drives with high-frequency current injection," *IEEE Transactions on Industry Applications*, vol. 50, no. 5, pp. 3295–3303, Sep. 2014.

[28] N. Bedetti, S. Calligaro, and R. Petrella, "Stand-still self-identification of flux characteristics for synchronous reluctance machines using novel saturation approximating function and multiple linear regression," *IEEE Transactions on Industry Applications*, vol. 52, no. 4, pp. 3083–3092, July 2016.

[29] M. Hinkkanen, P. Pescetto, E. Molsa, S. E. Saarakkala, G. Pellegrino, and R. Bojoi, "Sensorless self-commissioning of synchronous reluctance motors at standstill without rotor locking," *IEEE Transactions on Industry Applications*, vol. 53, no. 3, pp. 2120–2129, May 2017.

[30] R. E. Betz, R. Lagerquist, M. Jovanovic, T. J. Miller, and R. H. Middleton, "Control of synchronous reluctance machines," *IEEE Transactions on Industry Applications*, vol. 29, no. 6, pp. 1110–1122, 1993.

[31] L. Xu, X. Xu, T. A. Lipo, and D. W. Novotny, "Vector control of a synchronous reluctance motor including saturation and iron loss," *IEEE Transactions on Industry Applications*, vol. 27, no. 5, pp. 977–985, 1991.

[32] F. Leonardi, T. Matsuo, and T. Lipo, "Iron loss calculation for synchronous reluctance machines," in *Proceedings of International Conference on Power Electronics, Drives and Energy Systems for Industrial Growth*, vol. 1, Jan. 1996, pp. 307–312 vol.1.

[33] K. Yahia, D. Matos, J. O. Estima, and A. J. M. Cardoso, "Modeling synchronous reluctance motors including saturation, iron losses and mechanical

losses," in *Automation and Motion 2014 International Symposium on Power Electronics, Electrical Drives*, Jun. 2014, pp. 601–606.

[34] E. Rashad, T. Radwan, and M. Rahman, "A maximum torque per ampere vector control strategy for synchronous reluctance motors considering saturation and iron losses," in *Conference Record of the 2004 IEEE Industry Applications Conference, 2004. 39th IAS Annual Meeting.*, vol. 4, Oct. 2004, pp. 2411–2417 vol.4, iSSN: 0197-2618.

[35] J. Soltani, H. Abootorabi Zarchi, G. R. Arab Markadeh, and H. W. Ping, "Adaptive speed tracking control of three-Phase synchronous reluctance motor taking the iron loss resistance into account," in *2007 International Conference on Electrical Machines and Systems (ICEMS)*, Oct. 2007, pp. 625–630.

[36] A. Vagati, M. Pastorelli, and G. Franceschini, "High-performance control of synchronous reluctance motors," *IEEE Transactions on Industry Applications*, vol. 33, no. 4, pp. 983–991, 1997.

[37] e. a. Ion Boldea, "Distributed anisotropy rotor synchronous motor-identification and performance," in *Proceedings International Conference on Electrical Machines, Manchester, U.K., 15th-17th September 1992*. ICEM92 Secretariat, Department of Electrical Engineering and Electronics, UMIST, 1992, google-Books-ID: GPKBtgAACAAJ.

[38] D. Mingardi, M. Morandin, S. Bolognani, and N. Bianchi, "On the proprieties of the differential cross-saturation inductance in synchronous machines," *IEEE Transactions on Industry Applications*, vol. 53, no. 2, pp. 991–1000, 2017.

[39] A. Accetta, M. Cirrincione, M. Pucci, and A. Sferlazza, "Space-vector state dynamic model of the synchronous reluctance motor considering self, cross-saturation and iron losses," in *2021 IEEE Energy Conversion Congress and Exposition (ECCE)*, 2021, pp. 4164–4170.

[40] A. Accetta, M. Cirrincione, M. C. Di Piazza, G. La Tona, M. Luna, and M. Pucci, "Analytical formulation of a maximum torque per ampere (mtpa) technique for synrms considering the magnetic saturation," *IEEE Transactions on Industry Applications*, vol. 56, no. 4, pp. 3846–3854, May 2020.

[41] G. Ariaudo, "Valutazione sperimentale delle perdite nel ferro e controllo di massima efficienza per motori syr," Master's thesis, Politecnico di Torino, 2020.

[42] S.-G. Chen, F.-J. Lin, C.-H. Liang, and C.-H. Liao, "Development of FW and MTPV Control for SynRM via Feedforward Voltage Angle Control," *IEEE/ASME Transactions on Mechatronics*, vol. 26, no. 6, pp. 3254–3264, Dec. 2021.

[43] V. Manzolini, D. Da Rù, and S. Bolognani, "An Effective Flux Weakening Control of a SyRM Drive Including MTPV Operation," *IEEE Transactions on Industry Applications*, vol. 55, no. 3, pp. 2700–2709, May 2019.